RSC Advances

PAPER

View Article Online
View Journal | View Issue

Cite this: *RSC Adv.*, 2023, **13**, 9761

Enhancement of photovoltaic performance in ferrocenyl π-extended multi donor–π–acceptor (D–D′–π–A) dyes using chenodeoxycholic acid as a dye co-adsorbent for dye sensitized solar cells†

Selvam Prabu, [a] Thamodharan Viswanathan, [a] Ezhumalai David, [a] Sivanadanam Jagadeeswari[b] and Nallasamy Palanisami *[a]

A new set of multi-donor [ferrocene (D) and methoxyphenyl (D′)] conjugated D–D′–π–A based dyes [Fc–(OCH$_3$–Ph)C=CH–CH=CN–R{R=COOH (**1**) and C$_6$H$_4$–COOH (**2**)}] were synthesized as sensitizers for dye-sensitized solar cell (DSSC) applications. These dyes were characterized with the aid of analytical and spectroscopic techniques such as FT-IR, HR-Mass, and ^{1}H and ^{13}C NMR. The thermal stability of the dyes **1** and **2** were investigated using thermogravimetric analysis (TGA) and was found to be stable around 180 °C for dye **1** and 240 °C for dye **2**. The electronic absorption spectra for sensitizers display major bands between 400 and 585 nm that could be ascribed to an intramolecular charge transfer (ICT) between the electron donor and acceptor to create an efficient charge separation. The redox behaviour of the dyes was determined by cyclic voltammetry, which revealed the one-electron transfer from the ferrocene to ferrocenium ion ($Fe^{2+} \rightleftharpoons Fe^{3+}$), and potential was utilized to determine the band gap of the dyes (2.16 eV for **1** and 2.12 eV for **2**). Further, the carboxylic anchor dyes **1** and **2** have been utilized as photosensitizers in TiO_2-based DSSCs with and without co-adsorbance of chenodeoxycholic acid (CDCA), and the photovoltaic performances were studied. The obtained photovoltaic parameters of dye **2** are open-circuit voltage (V_{oc}) = 0.428 V, short-circuit current density (J_{sc}) = 0.086 mA cm^{-2}, the fill factor (FF) = 0.432 and the energy efficiencies (η) = 0.015%, the overall power conversion efficiencies were found to be increased in the presence of CDCA as a co-adsorbent. The photosensitizers with the addition of CDCA show higher efficiencies compared to those in the absence of CDCA, which can prevent the formation of aggregation and increased electron injection of the dyes. Among the dyes, the 4-(cyanomethyl) benzoic acid (**2**) anchor showed higher photovoltaic performance compared with the cyanoacrylic acid (**1**) anchor due to the introduction of additional π-linkers and acceptor unit, which enables the lowering of the energy barrier and charge recombination process. In addition, the experimentally observed HOMO and LUMO values were in good agreement with the theoretical calculation by the DFT-B3LYP/6-31+G**/LanL2TZf level of theory.

Received 20th October 2022
Accepted 7th March 2023

DOI: 10.1039/d2ra06615g

rsc.li/rsc-advances

1 Introduction

One of the most promising alternative sources of low-cost renewable energy in the future is expected to be dye-sensitized solar cells (DSSCs) and they have been identified as the first reported by O'regan and Grätzel in 1991.[1–3] The design and fabrication of DSSCs as a novel form of photovoltaic technology is attracting enormous attention from chemists and material scientists. The development of photo-sensitizers has achieved significant progression, with photon-to-current established power conversion efficiencies of 11.4% to 14.3%.[4,5] To achieve higher efficiencies, the sensitizers are important constituents in DSSCs, because they regulate the light harvesting and charge separation properties.[1–3] Furthermore, the structural changes of sensitizers can improve their molar extinction coefficient and solar light harvesting ability. This can be attained by altering the chromophore and anchoring groups, which enhance the photocurrent and effectiveness of the DSSCs.[5–7] Several metal based sensitizers such as Ru-based dyes,[8–10] Zn porphyrins,[11] and perovskites[12,13] have been reported, which show significant power conversion efficiency (PCE). However, these devices have limited uses in the real-world implementation due to their high cost, particularly the Ru-based dyes. To restrain this techno-

[a]*Centre for Functional Materials, Department of Chemistry, School of Advanced Sciences, Vellore Institute of Technology, Vellore 632014, Tamilnadu, India. E-mail: palanisami.n@gmail.com; palanisami.n@vit.ac.in; Tel: +91 98426 39776*

[b]*Clean Energy Lab, Department of Chemistry, Indian Institute of Technology Madras, Chennai 600036, India*

† Electronic supplementary information (ESI) available. See DOI: https://doi.org/10.1039/d2ra06615g

economic problem, several organic dyes have also been utilized as sensitizers in DSSC. Organic dyes like triphenylamine (TPA) donors and different π-conjugated linkers such as aromatic and heteroaromatic moieties with cyanoacrylic acid as an anchoring and acceptor group have been explored as sensitizers.[14–16] However, due to ineffective charge-transfer capabilities, these organic dyes are unable to convert solar energy into electrical energy.

In the last two decades, researchers have developed the ferrocene based complexes for DSSC applications, owing to the versatile oxidation states of iron ($Fe^{2+} \rightleftharpoons Fe^{3+}$) in ferrocene moiety, promoting reversible one-electron redox reaction, which act as a donor in DSSCs, and redox potential of the dyes can be tuned by varying the substitution on cyclopentadienyl ring.[17–19] Moreover, ferrocene shows the lower absorbance between 440 and 480 nm as well as at higher energy (250, 300 and 360 nm) and this lowest energy might be suitable as sensitizers for DSSCs applications.[18] The lowest energy can be shifted to infrared region by substituting acceptor unit of carboxylic acid groups, which also act as anchoring group in DSSCs.[20] In these aspects, ferrocenyl derivatives have been utilized in DSSC as possible photosensitizers. In particular, homo and heteroleptic based dithiocarbamate complexes (Ni, Pt and Cu),[21,22] triphenylamine based donor–acceptor dyes,[23] porphyrin derivatives,[24] diketopyrrolopyrrole based acceptors,[25] benzimidazole[26] and biferrocenyl quinoxaline[27] with different anchors have been investigated on photovoltaic performances. In addition, Cariello *et al.* studied the influence of π-conjugation in ferrocene molecules on DSSC performances. The π-conjugation played an essential role in regulating their optical and redox properties.[28] Recent studies have shown that the acceptor substituent coupled to the cyclopentadienyl ring, which increases the formal redox potential of the ferrocene molecule. Hence, the redox potential of this sandwich moiety controlled for DSSC applications.[18,19]

To enhance the DSSC performance, different types of additives have been added into dye solutions as a co-adsorbent. The commonly used co-adsorbent is chenodeoxycholic acid (CDCA), which can act as a hydrophobic spacer and prevent the formation of aggregation, when the dye was tightly packed with monolayer and it gives relatively better surface coverage and effectively hindering the back-electron transfer from conduction band of TiO_2 to electrolyte (iodide/triiodide). As a result, the improving the DSSC performance by enhancement of open circuit voltage of the device.[29] In this aspect, some of us have explored an organic dyes such as ethynyl-pyrene substituted phenothiazine[30] and starburst configured imidazole-arylamine[31] as sensitizers, which is subjected to DSSC studies with or without co-adsorbents, and the results are relatively higher photo conversion efficiency (PCE) in the presence of CDCA co-adsorbents.[30,31] In the literature, reports were available for donor–π–acceptor organic sensitizers with CDCA co-adsorbent,[29–31] but ferrocenyl based systems were yet to be reported.

Keeping the aforementioned aspects in mind, we have developed new π-extended methoxyphenyl conjugated ferrocenyl multi-donor dye as photosensitizers. The introduction of methoxyphenyl (D′) in ferrocene (D) moiety acts as an additional donor, results enhanced the charge transfer process. Recently some of us studied the ferrocenyl multi-donor systems for nonlinear optics and luminescent properties.[32] To the best of our knowledge, the ferrocenyl sensitizers with co-adsorbent CDCA in DSSCs yet to be reported. The ferrocenyl multi-donor coupled with strong acceptors like cyanoacrylic acid and 4-(cyanomethyl) benzoic acid, which can be used as sensitizers in DSSCs and their electron withdrawing effects have been utilized to develop charge-transfer process.[33–35] In this expedition, we have synthesized new D–π–A type of ferrocenyl methoxyphenyl-substituted acids and tested their ability for sensitizers in DSSCs. In addition, we have done the theoretical calculations using density functional theory (DFT/TD-DFT) using B3LYP/6-31+G(d,p)/LanL2TZf level of theory and these results were correlated with experimental calculations.

2 Experimental sections

2.1 Materials and methods

All the chemicals were purchased from Sigma Aldrich and TCI Chemical Co. The solvents were used after purified by distillation. The column chromatography was carried out using silica gel 60 (AVRA, 100–120 mesh).

2.2 General physical measurements

The NMR spectra were recorded on a BRUKER (400 MHz) spectrometer with $CDCl_3$ and DMSO-d_6 as a solvent and tetramethyl silane as an internal standard and the chemical shifts are reported in δ (ppm). The HR-Mass spectra were recorded using WATERS–XEVO G2-XS-QToF High Resolution Mass Spectrometer (HRMS) using ESI method. The elemental analysis was carried out using CHNS Elemental Analyzer-Perkin Elmer-2400 CHNS/O Series. FT-IR spectra were obtained using a SHIMADZU IR Affinity-1 instrument equipped with a high-sensitivity DLATGS detector with KBr discs. The Electronic absorption spectra were recorded using a JASCO UV-visible spectrometer in a 1 cm^2 quartz cuvette at room temperature using dichloromethane as a solvent. The cyclic voltammogram of the chromophore was carried out on a CH-Instruments Model CHI620E in acetonitrile solvent (1×10^{-3} M) that containing 0.1 M tertbutyl ammonium perchlorate as supporting electrolyte at the scan rate 0.1 V s^{-1}. A platinum wire was used as a counter electrode, glassy carbon as the working electrode and reference electrode as a saturated Ag/AgCl. Thermo gravimetric analysis was done by TGA SDT Q 600 V20.9 Build 20 instrument under N_2 atmosphere at heat rate 20 °C min^{-1} (0–800 °C).

2.3 Synthesis of dyes

The 3,3(4-methoxyphenyl) ferrocenyl acrylaldehyde was synthesized according to the reporting procedure.[32,36] The dyes **1** and **2** were synthesized by Knoevenagel condensation reaction.[32] The 3,3(4-methoxyphenyl) ferrocenyl acrylaldehyde (1 mmol, 0.214 g), 1 mmol of substituted acetonitrile (2-cyanoacetic acid (**1**) or 4-(cyanomethyl) benzoic acid (**2**)) and

piperidine (0.1 ml) in methanol (10 ml) were kept under reflux for 6 hours. After completing the reaction, the solvent was evaporated and made a crude. Then the crude was purified by column chromatography using hexane and ethyl acetate (8 : 2) as eluent to attain the ferrocenyl dyes.

2.4 Characterization data

2.4.1 3,3(4-Methoxyphenyl) ferrocenyl acrylaldehyde. 3-Chloro-3-ferrocenylacrylaldehyde (1 mmol, 0.274 g) and *p*-methoxy phenylboronic acid (1 mmol, 0.151 g). Dark red colour solid, yield: 348.5 mg, 82%. Mp. = 128–132 °C (decomposed). Elemental analyses for CHN ($C_{20}H_{18}FeO_2$): Calcd. C, 69.39; H, 5.24; found C, 69.07, H, 5.10%. HRMS for ($C_{20}H_{18}FeO_2$) (*m*/*z*): Calcd. 346.0656, found mass: 346.0661. ^{1}H NMR (400 MHz, $CDCl_3$) δ (ppm): 9.37 (d, J = 8.4 Hz, 1H, CHO), 7.346 (d, J = 8.8 Hz, 2H, C_6H_4), 6.98 (d, J = 8.8 Hz, 2H, C_6H_4), 6.50 (d, J = 8 Hz, 1H, CH), 4.50 (s, 2H, H_α C_5H_4), 4.44 (s, 2H, H_β C_5H_4), 4.15 (s, 5H, C_5H_5), 3.89 (s, 3H, OCH_3). ^{13}C NMR (100 MHz, $CDCl_3$) δ (ppm): 193.1 (1C, C═O), 165.5 (1C, C–OCH_3), 160.2 (1C, *p*-C, C_6H_4), 130.9 (2C, *m*-C, C_6H_4), 128.7 (1C, CH), 124.2 (1C, CH), 113.5 (2C, *o*-C, C_6H_4), 82.1 (1C, C-1, C_{ipso} C_5H_4), 71.7 (2C, C_β C_5H_4), 70.3 (5C, C_5H_5), 69.2 (2C, C_α C_5H_4), 55.4 (1C, OCH_3).

2.4.2 Dye 1. 3,3-(4-Methoxyphenyl) ferrocenyl acrylaldehyde (1 mmol, 0.346 g) and 2-cyanoacetic acid (1 mmol, 0.085 g). Dark green colour solid, yield: 367.5 mg, 84%. Mp. = 256–261 °C (decomposed). Elemental analyses for CHN ($C_{23}H_{19}FeNO_3$): Calcd. C, 66.85; H, 4.63; N, 3.39; found C, 66.87, H, 4.70, N, 3.41%. HRMS for ($C_{23}H_{19}FeNO_3$) (*m*/*z*): Calcd. 413.0714, found mass: 413.0716. ^{1}H NMR (400 MHz, $CDCl_3$) δ (ppm): 7.79 (d, J = 12 Hz, 1H, CH), 7.24 (d, J = 8 Hz, 2H, C_6H_4), 7.11 (d, J = 16 Hz, 1H, CH), 6.99 (s, J = 8 Hz, 2H, C_6H_4), 4.61 (s, 2H, H_α C_5H_4), 4.54 (s, 2H, H_β C_5H_4), 4.18 (s, 5H, C_5H_5), 3.90 (s, 3H, OCH_3). ^{13}C NMR (100 MHz, $CDCl_3$) δ (ppm): 168.5 (1C, C═O), 166.2 (1C, C–OCH_3), 160.6 (1C, *p*-C, C_6H_4), 154.5 (1C, CH), 130.9 (2C, *m*-C, C_6H_4), 125.2 (1C, CH), 119.1 (1C, C≡N), 113.8 (2C, *o*-C, C_6H_4), 98.2 (1C, C–CN), 83.3 (1C, C-1, C_{ipso} C_5H_4), 73.3 (2C, C_β C_5H_4), 71.2 (5C, C_5H_5), 70.4 (2C, C_α C_5H_4), 55.5 (1C, OCH_3). FT-IR (KBr): 3439 (b) ν(OH), 3093 (w) ν(C–H arom), 2929 (w) ν(C–H aliph), 2839 (w) ν(OCH_3), 2214 (s) ν(C≡N), 1708 (s) ν(C═O), 1604 (s), 1575 (s), 1510 (s), 1452 (s), 1388 (s), 1369 (s), 1311 (s), 1249 (s) ν(C═C), 1219 (s), 1190 (s), 1107 (m) ν(C═C Fc), 1028 (s) ν(C–O), 970 (m), 950 (s), 835 (m) ν(C–C Fc), 783 (s) ν(C–H arom), 648 (m), 493 (s) cm^{-1}. UV-visible data λ_{max} (CH_2Cl_2) = 241 (π–π*), 389 (n–π*) and 584 (d–d) nm, and molar extinction coefficient ε_{max} = 9975, 11 840 and 2905 M^{-1} cm^{-1}.

2.4.3 Dye 2. 3,3-(4-Methoxyphenyl) ferrocenyl acrylaldehyde (1 mmol, 0.346 g) and 4-(cyanomethyl) benzoic acid (1 mmol, 0.161 g). Dark green colour solid, yield: 367.5 mg, 75%. Mp. = > 300 °C (decomposed). Elemental analyses for CHN($C_{29}H_{23}FeNO_3$): Calcd. C, 71.18; H, 4.74; N, 2.86%; found C, 71.07, H, 4.34, N, 2.93%. HRMS for ($C_{29}H_{23}FeNO_3$) (*m*/*z*): Calcd. 489.1027, found mass: 489.1021. ^{1}H NMR (400 MHz, DMSO-d_6) δ (ppm): 7.97 (s, 2H, C_6H_4), 7.54 (s, 2H, C_6H_4), 7.37 (d, J = 8.4 Hz, 2H, C_6H_4), 7.32 (d, J = 11.7 Hz, 1H, CH), 7.15 (d, J = 11.7 Hz, 1H, CH), 7.09 (d, J = 8.4, 2H, C_6H_4), 4.56 (s, 2H, H_α C_5H_4), 4.45 (s, 2H, H_β C_5H_4), 4.22 (s, 5H, C_5H_5), 3.85 (s, 3H, OCH_3). ^{13}C NMR (100 MHz, DMSO-d_6) δ (ppm): 160.0 (1C, C═O), 156.2 (1C, C–OCH_3), 141.7 (1C, CH), 131.3 (4C, *m*-C C_6H_4), 120.5 (2C, *p*-C C_6H_4 & CH), 117.8 (1C, C≡N), 114.2 (4C, *o*-C, C_6H_4), 107.7 (1C, CH), 84.3 (1C, C_{ipso} C_5H_4), 71.6 (2C, C_β C_5H_4), 70.6 (5C, C_5H_5), 69.0 (2C, C_α C_5H_4) and 55.6 (1C, OCH_3). FT-IR (KBr): 3433 (b) ν(OH), 3091 (w) ν(C–H arom), 2926 (w) ν(C–H aliph), 2852 (w) ν(OCH_3), 2208 (s) ν(C≡N), 1691 (s) ν(C═O), 1606 (s), 1575 (s) ν(C–C), 1564 (s), 1510 (s), 1415 (s), 1276 (s) ν(C═C), 1156 (w), 1247 (s), 1178 (s), 1107 (s) ν(C═C Fc), 1031 (s) ν(C–O), 954 (w), 833 (s) ν(C–C Fc), 781 (s) ν(C–H arom), 698 (m), 528 (m), 495 (s) cm^{-1}. UV-visible data λ_{max} (CH_2Cl_2) = 242 (π–π*), 410 (n–π*) and 573 (d–d) nm, and molar extinction coefficient ε_{max} = 12 147, 15 562 and 4140 M^{-1} cm^{-1}.

2.5 Fabrication and characterization of DSSCs

FTO glass obtained from GreatCell Solar (MS001695-10) was cut into 2 × 1.5 cm sized plates, which were immersed into detergent solution for 10 min. Detergent removed the organic/greasy matter on FTO plate. Then, distilled water, acetone and isopropyl alcohol cleanings were performed (each 20 min) while sonicating the FTO plate in the solvents. At the end, the cleaned FTO plates were dried in vacuum oven at 80 °C. This plate was dip coated with 40 mM aq. $TiCl_4$ solution at 70 °C for 30 min. After repeating dip coating procedure for 2 more times, the plate was annealed at 500 °C for 30 min in air oven. $TiCl_4$ dip coating is mainly performed to avoid direct contact of electrolyte of DSSC with the FTO. Upon annealing, $TiCl_4$ transforms into a transparent TiO_2 layer. A scotch tape having circular hole of 0.196 cm^2 area was stuck on the surface of dip coated TiO_2. This circular hole was filled with 20 nm sized TiO_2 particles applying TiO_2 paste by doctor blade technique. Upon drying the TiO_2 paste at 70 °C, and after peeling off the scotch tape, it was subjected to annealing at 500 °C for 30 min to realize a transparent TiO_2 layer of 6 μm thick (as measured by profilometer). On this a scattering layer of TiO_2 of 5 μm thick was applied by doctor blade technique, which was sintered at 400 °C for 30 min to form a light reflecting layer. After cooling to 70 °C, the plate was immersed into 0.5 mM ferrocene dye in acetonitrile: *t*-butyl alcohol (1 : 1, v/v) solution and kept at 25 °C for 12 h for adsorbing dye onto TiO_2 surface. The photoanode was taken out of the dye bath and was rinsed with anhydrous acetonitrile to dislodge any unadsorbed dye onto the electrodes. A 0.5 mm thick platinum sheet and photoanode were superimposed on each other having a hot melt polymer film as gasket between the two electrodes. The gap between the photoanode and platinum sheet was filled with I^-/I_3^- electrolyte. The electrolyte is made of 0.05 M, 0.1 M, 0.6 M and 0.5 M of iodine, lithium iodide, 1-butyl-3-methylimidazolium iodide, and *t*-butyl pyridine, respectively in 15 : 85 v/v % of valeronitrile and acetonitrile mixed solvent.

2.6 Theoretical calculations

The electronic structure and molecular properties of the dyes **1** and **2** were investigated using density functional theory (DFT) and time-dependent density functional theory (TD-DFT) to understand the bonding patterns, electronic charge and molecular orbital energy distributions. The optimization of the

molecular geometries leading to energy minima was achieved using the DFT [with Becke's three parameter exchange and the Lee-YangParr's correlation functional (B3LYP)] with 6-31+G(d,p) basis set for C, O and H atoms and LanL2TZf functional for Fe, under vacuum.[37,38] As noted above, this DFT method appeared in benchmark calculations for the B3LYP/6-31+G(d,p)/LanL2TZf parent ferrocene.[39] Also, the time dependent density functional theory (TD-DFT) at 6-31+G(d,p) has been employed in HOMO–LUMO energies, oscillator strengths, absorption wavelengths λ_{max}. All computation calculations were carried out using the GAUSSIAN 16 package.[40] The frontier molecular orbital structures and electronic geometries were taken by Gauss View 6.1.[41]

3 Result and discussion

3.1 Synthesis

The ferrocenyl based acid dyes **1** and **2** were synthesized by the reaction between substituted acetonitrile (2-cyanoacetic acid (**1**) or 4-(cyanomethyl) benzoic acid (**2**)) in the presence piperidine and methanol as a solvent to form dyes **1** and **2**, as shown in Scheme 1. The synthesized dyes were characterized by FT-IR, ^{1}H and ^{13}C NMR and HR-Mass spectroscopic methods.

3.2 Characterization of dyes

The purity of dyes has been examined using ^{1}H and ^{13}C NMR spectroscopy techniques and were recorded in and $CDCl_3$ (for acrylaldehyde and dye **1**) DMSO-d_6 (for dye **2**) at room temperature using TMS as an internal standard and the spectra were displayed in Fig S1–S6.† The ^{1}H NMR spectra of dyes showed that the methoxy protons are appearing at 3.8 ppm as a singlet. The ferrocene protons are resonating in the region of 4–5 ppm. The ferrocene protons of unsubstituted cyclopentadienyl ring (η^5-C_5H_5) are appeared as a singlet in the region of 4.2 ppm and substituted cyclopentadienyl ring (η^4-C_5H_4) assigned at 4.4 and 4.6 ppm. The methoxy substituted aromatic protons are assigned at 7.0 to 7.3 ppm. In the case of dye **2**, acid group attached aromatic ring protons are resonating in the range of 7.5 to 7.9 ppm. The ^{13}C NMR spectra of dyes show that the Fc-CH carbon resonates at 69.24–79.73 ppm, –C=O carbon resonates at 160.0 ppm and 168.5 ppm and then the –C≡N carbons are assigned at 119.1 (**1**) and 117.8 (**2**) ppm, respectively. The mass spectra of the dyes **1** and **2** were showed a peak with the expected isotopic pattern at m/z = 346.0661 (for acrylaldehyde), 413.0716 (for dye **1**) and 489.1021 (for dye **2**), respectively, and the obtained data coincided with calculated data as shown in Fig. S7–S9.† The FT-IR spectra of dyes **1** and **2** were shown in Fig. S10,† the broad –OH stretching of both the dyes **1** and **2** were found around 3430 cm^{-1}, it was identified the formation of carboxylic acid group. The –CN stretching vibrations of dyes were observed at 2205 cm^{-1} and the bands around 1700 cm^{-1} were seen due to –C=O stretching. The –OCH_3 stretching vibration of dyes were observed at 2841 cm^{-1}. Moreover, the aliphatic and aromatic –CH vibrations were observed around 2920 cm^{-1} and 3080 cm^{-1}, respectively. In addition, the thermal stability of the dyes **1** and **2** were studied using thermogravimetric analysis (TGA) at the heating rate of 20 °C min^{-1} up to 800 °C, and it shows that the dyes **1** and **2** were stable around 180 °C and 240 °C, respectively (Fig. S11†).

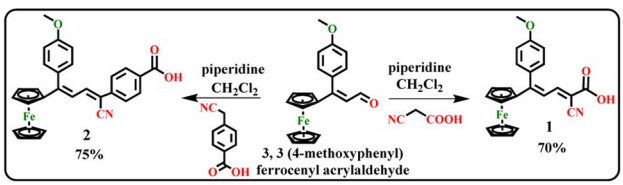

Scheme 1 Synthetic route of dyes **1** and **2**.

3.3 Optical properties of dyes

The absorption spectra of the dyes were performed in dichloromethane solution and the spectra show three absorption band as shown in Fig. 1. The higher energy absorptions are observed at the region of 241 and 242 nm which is due to π–π* transition and originated to a ligand-centered transition. The absorption bands at 389 for dye **1** and 410 nm for dye **2** shows the medium energy due to the *n*–π* transition that can be described by metal-to-ligand charge transfer (MLCT) or ligand-to-metal charge transfer (LMCT) due to intramolecular charge transfer (ICT).[42] The absorption band at 564 and 548 nm occurs d–d transition (assigned to $^1E_{1g} \leftarrow {}^1A_{1g}$), this low energy transition is due to the degenerate transition of Fe(II) for metal–ligand charge transfer (dπ–π*).[43] Meanwhile, these spectra were compared with ferrocene and the wavelength was quite red shifted. The extensive π-conjugation that occurs from the ferrocene to the aromatic system *via* the phenyl and diene linkage, which results in significant electrical communication in the molecule, may be a causing for the bathochromic shifts. This important red shift in the electronic absorption band corresponding to ferrocene, which promote these molecules are used as potential sensitizers in DSSC.[44] The absorption spectra of dyes **1** and **2** adsorbed on a transparent TiO_2 film around 6 mm thick are displayed in Fig. 2. The lower energy absorption wavelength of dyes **1** and **2** are 551 nm and 539 nm, respectively and it indicates slight blue shift, which may be an electronic coupling of the dyes on the TiO_2 surface.[45]

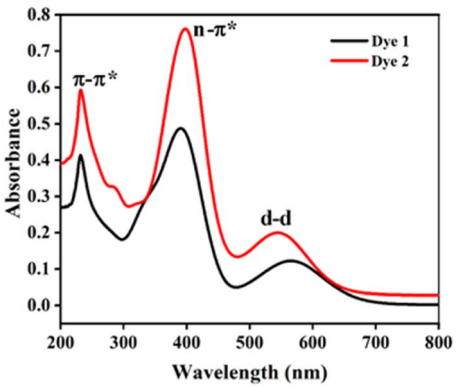

Fig. 1 Absorption spectra of dyes **1** and **2** in CH_2Cl_2 solution (1×10^{-5} M).

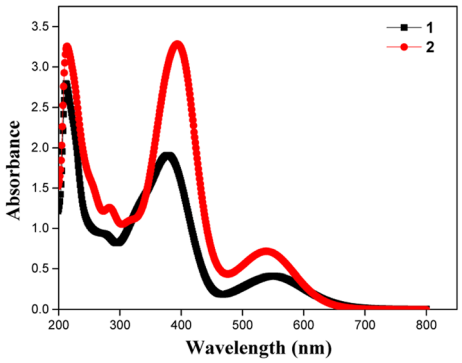

Fig. 2 Electronic absorption spectra of the dyes **1** and **2** adsorbed on TiO_2 film.

The diffuse reflectance spectra (DRS) of the dyes **1** and **2** were calculated and the observed wavelength was around 200–2500 nm. This spectrum was useful to understand the optical absorption or transmittance window and cut-off wavelength of the dyes. The charge transfer involving in the dyes **1** and **2** were 350–1650 nm, which indicates that the absorption takes place in visible region as shown in Fig. 3.

The absorption co-efficient (α) was calculated by the Kubelka–Munk eqn (1).[46]

$$(\alpha/S) = (1 - R)2/2R \quad (1)$$

where, R is the diffused reflectance at certain energy, α is an absorption coefficient and S is the scattering coefficient which was situated at the localized states near the mobility edges according to Mott and Davis model of the density of states.

The optical energy gap (E_g) was calculated using the following eqn (2).[47]

$$(\alpha\hbar\nu)^2 = A(\hbar\nu - E_g) \quad (2)$$

where, A is a constant, $\hbar$ is Plank's constant, α is absorption coefficient and ν is the frequency of incident photons.

The optical energy gap (E_g) of the investigated dyes **1** and **2** were plotted $(\alpha\hbar\nu)^2$ *versus* photon energy ($\hbar\nu$) using the Tauc's relationship as shown in Fig. 4. The band gap of the dyes **1** and **2** were found to be 3.23 eV (**1**) and 3.08 eV (**2**). The obtained band gap in DRS in the UV region is due to the strong interactions of the molecules in the solid state, which limit the efficient charge transfer. Moreover, the DFT was carried out in both gas and solution phase, it results the red shift in visible region due to the effective charge transfer process. In addition, the both DRS and theoretically calculated energy and band gap values follow the same trend for the dyes **1** and **2**.

3.4 Electrochemical properties of dyes

The electrochemical behavior of the dyes **1** and **2** were performed in dichloromethane solution, containing 0.1 M tetrabutylammonium perchlorate (TBAP) as a supporting electrolyte at a scan rate of 100 mV s^{-1}. The platinum wire acts as a counter electrode, glassy carbon as a working electrode and Ag/AgCl electrode as a reference electrode. The cyclic voltammogram of dyes as shown in Fig. 5, and the electrochemical data were summarize in Table 2. The current ratio was (i_{pa}/i_{pc}) equal to unity and it is exhibits quasi-reversible for the electrochemical assessment. The redox potentials of the dyes **1** and **2** were observed in the range of 641–832 mV and it indicates the one-electron charge transfer from ferrocene to ferrocenium ion ($Fe^{2+} \rightleftharpoons Fe^{3+}$). The observed half-wave potential ($E_{1/2}$) of dyes **1** and **2** were shows higher half-wave potential ($E_{1/2}$ = 755 for **1** and 742 mV for **2**) and peak separation (ΔE = 153 for **1** and 108 mV for **2**) values than the parent ferrocene ($E_{1/2}$ = 443.5 mV and ΔE = 71 mV for FcH/FcH+ reversible system).[48] This implies that dyes are shifted towards right hand side due to the substituted carboxylic groups as shown in Fig. 5. In addition, it is necessary to know highest occupied molecular orbital (HOMO) and lowest unoccupied molecular orbital (LUMO) energy levels. These parameters are useful for photosensitizer of regeneration dyes and the electron transfer process in DSSCs.[26,49] The HOMO and LUMO energy level were derived by the formula $E_{HOMO} = -(E_{ox} + 4.4)$ and ELUMO = $(E_g^{optical} + E_{HOMO})$.[32]

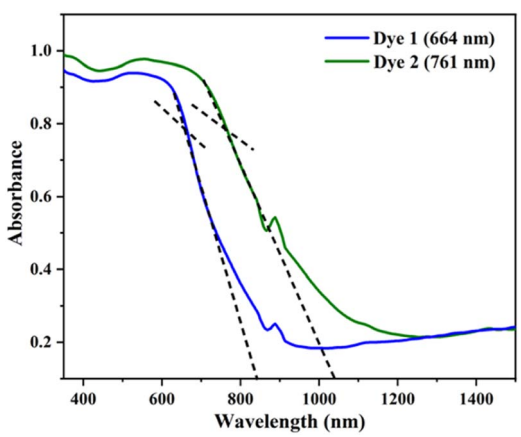

Fig. 3 Diffuse reflectance spectra of the dyes **1** and **2**.

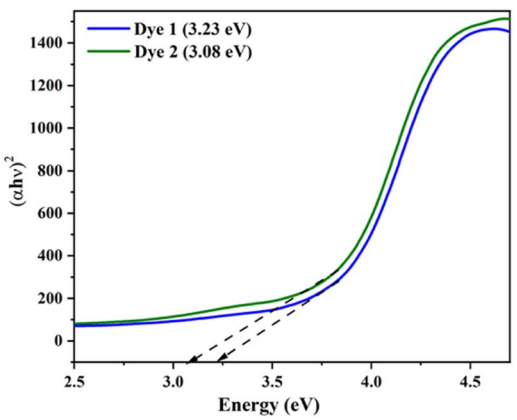

Fig. 4 Tauc's plots of $(\alpha\hbar\nu)^2$ *versus* photon energy ($\hbar\nu$) of the dyes **1** and **2**.

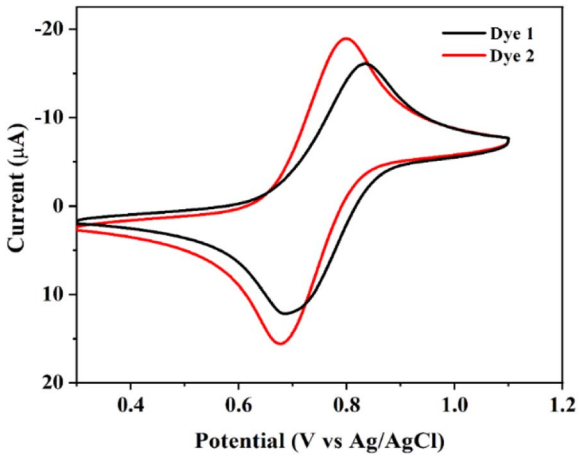

Fig. 5 Cyclic voltammogram of dyes **1** and **2** in the presence of 0.1 M TBAP supporting electrolyte at 0.1 mV s^{-1} in 10^{-3} M CH_2Cl_2 solution.

3.5 DFT and TD-DFT calculations

The density functional theory (DFT) was used to analyze the molecular geometries and electronic properties of the ferrocene conjugated multi-donor dyes **1** and **2**. The single crystal data of the dyes were not obtained due to the poor diffraction quality. The synthesized dyes were optimized in the gas phase and the geometrical parameters were determined by B3LYP/6-31+G(d,p)/LanL2TZf. For transition metal, this DFT method appeared in benchmark calculations for the B3LYP/6-31+G(d,p)/LanL2TZf parent ferrocene and is known to produce reasonably accurate geometries[39] and the molecular geometries of the dyes **1** and **2** were shown in Fig. 6. The optimized structure has accurate geometry with previously reported structure.[32,34]

To understand the molecular electronic structure of the dyes **1** and **2**, we have calculated the molecular electrostatic potential (MEP), as shown in Fig. 7. It is used to predict the reactivity of molecular species, where the approaching nucleophile or electrophile is attracted to a positive or negative region of the molecule.[50] In MEP plot, the maximum positive and negative potentials have been indicated by blue and red with slightly yellow surface respectively as shown in Fig. 7, and it gives the information about molecular size and shape along with positive, negative and neutral electrostatic potential of the dyes **1**

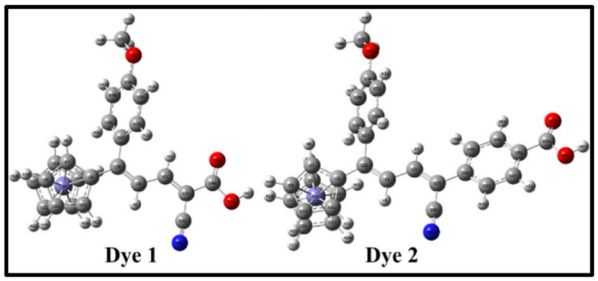

Fig. 6 The optimized geometries of the dyes **1** and **2** obtained at B3LYP/6-31+G(d,p)/LanL2TZf level of theory.

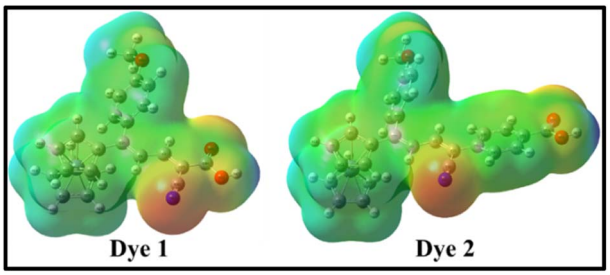

Fig. 7 The molecular electrostatic potential maps for the dyes **1** and **2** obtained at B3LYP/6-31+G(d,p)/LanL2TZf level of theory.

and **2**. The blue colour stands for nucleophilic attacks, which illustrates the considerable positive potential of the –OH group in dyes **1** and **2**. The cyano (–C≡N) and carbonyl (–C=O) group show maximum negative potential that was denoted by red with slightly yellow surface, which is preferred for electrophilic attacks.

The highest occupied molecular orbital (HOMO), lowest unoccupied molecular orbital (LUMO) energies and absorption maxima (λ_{max}), were calculated using B3LYP/6-31+G(d,p)/LanL2TZf level of theory,[37–39] and the values were reported in Table 1. Based on the computed results, it is clear that the HOMO and LUMO orbital distribution developed through the charge exchange from the ferrocenyl donor to acceptor unit. In the dyes **1** and **2**, the electronic distribution of the HOMO is strongly localized over the ferrocene and π-conjugation double bond of the dyes and partially localized on methoxy substituted phenyl ring. The calculated HOMO energy levels are **1** (−5.89 eV) and **2** (−5.59 eV), respectively. The LUMO is mainly constituted by the acceptor moieties and π-conjugation of a double bond in the chromophores. In contrast, the LUMO energy levels are −2.77 eV (for **1**) and −2.99 eV (for **2**). The obtained energy gap of the dyes are 3.12 eV (**1**) and 2.60 eV (**2**). The HOMO and LUMO energy levels are shown in Fig. 8. Here, we have observed that the π-spacer double bonds were contributed in HOMO as well as LUMO levels, and it contributes for the balanced charge transfer[32] of dyes **1** and **2**. In both the dyes, considerable overlap of the frontier orbital arises, which indicates an efficient ICT from the donor to the terminal acceptor group that anchors to the TiO_2 surface.[51]

Further, we have carried out the time-dependent density functional theory (TD-DFT) using B3LYP/6-31+G(d,p)/LanL2TZf method for the dyes **1** and **2** to assign the definite transition observed in the experiments (Table 1). The theoretical UV-visible spectra were shown in Fig. S12† and the major transitions of n–π* transition was observed to be an intramolecular charge transfer transition which followed the same trend with experimentally observed results. The theoretically observed higher energy transition with higher intense band at 497 nm (**1**) and 513 (**2**), corresponds to HOMO-2 → LUMO excitations (more than 65%). This excited state with large oscillator strengths can be assigned as $n \rightarrow \pi^*$ due to the electronic transition within the molecules. The lower-energy (LE) transition with less intense band at 699 nm (**1**) and 640 nm (**2**) is

Table 1 UV-visible absorption and DRS optical band gap data

Dyes	λ_{max}^{HE} [a] [nm (eV^{-1})] ε^{a} ($\times 10^3$) [M^{-1} cm^{-1}]	λ_{max}^{ME} [a] [nm (eV^{-1})] ε^{a} ($\times 10^3$) [M^{-1} cm^{-1}]	λ_{max}^{LE} [a] [nm (eV^{-1})] ε^{a} ($\times 10^3$) [M^{-1} cm^{-1}]	λ_{max} [b] (nm eV^{-1})	DRS optical energy gap[c] (eV)
1	241(5.10)/9.6	389(3.17)/17.4	564(2.19)/4.3	475/2.61	3.23
2	242(5.10)/10.3	410(3.10)/16.3	548(2.26)/5.0	417/2.97	3.08

[a] UV-visible, HE = Higher Energy, ME = Medium Energy, LE = Lower Energy. [b] TD-DFT values. [c] Optical energy gap from DRS-UV [$(\alpha\hbar\nu)2$ *versus* $(\hbar\nu)$].

Table 2 Cyclic voltammetry data and experimental HOMO, LUMO and optical band gap

Dyes	E_{pa} [a] (mV)	E_{pc} [a] (mV)	i_{pa}/i_{pc}	$E_{1/2}$ [a] (mV)	ΔE^{a} (mV)	E_{HOMO} [a] (eV)	E_{LUMO} (eV)[a]	λ^{onset} (nm)[b]	$E_g^{opticalc}$ (eV)
Dye **1**	832	679	1.2	755	153	−5.08	−2.96	584	2.12
Dye **2**	796	688	1.1	742	108	−5.05	−2.89	573	2.16

[a] Calculated as HOMO and LUMO level obtained from cyclic voltammetry using EHOMO = $-(E_{ox}^{onset} + 4.4)$. $E^{optical}$ onset values obtained from oxidation peak in cyclic voltammogram. ELUMO = $E_g^{optical}$ + EHOMO. [b] Calculated as λ^{onset} values from absorption spectra in CH_2Cl_2 solvent. [c] Calculated as optical band gap calculated from absorption onset/edge using the equation e $(E_g^{optical}) = 1240/\lambda^{onset}$.

mainly described by HOMO → LUMO excitations (more than 58%), such excitations were dominated by one-electron transition with a large transition dipole moment. The electronic structures, excited energies, oscillator strengths and orbital transitions of the dyes **1** and **2** are listed in Tables S2 and S3.†

3.6 DSSC studies

To study the photovoltaic performance of the DSSCs fabricated dyes **1** and **2**, the *J*–*V* curves were recorded. The newly synthesized ferrocenyl multi-donor–π–acceptor dyes **1** and **2** were employed as additives in DSSCs. Because these dyes having –OH group, which provides superior anchorage on the TiO_2 surface, thereby leading to a better photon absorption for current conversion. In dye-sensitized solar cells, the ability to generate electricity is determined by various components, such as TiO_2, dyes, iodide/triiodide concentrations, and Pt surfaces. The current voltage (*J*–*V*) curves are shown in Fig. 9 with (A) and without co-adsorbent (B) under 1 sun condition. The corresponding photovoltaic parameter of the open-circuit voltage (V_{oc}), short-circuit current density (J_{sc}), the fill factor (FF) and the power conversion efficiencies (η) are summarized in Table 3. The obtained energy efficiencies of dyes **1** and **2** were 0.0017% (**1**) and 0.0047% (**2**) in absence of the co-adsorbent [J_{sc} = 0.025 mA cm^{-2} (**1**) and 0.049 mA cm^{-2} (**2**), V_{oc} = 0.211 V (**1**) and 0.282 V (**2**) and FF = 0.318 (**1**) and 0.347 (**2**)]. The lower efficiencies were observed in the both dyes **1** and **2**, due to the aggregation and poor adsorption on TiO_2 surface. In order to reduce the aggregation chenodeoxycholic acid (CDCA) as co-adsorbent was added at the concentration of 10 mM.[52] This resulted in the overall power conversion efficiencies were found to be increased η = 0.012% (**1**) and 0.015% (**2**), respectively, [J_{sc} = 0.071 mA cm^{-2} (**1**) and 0.086 mA cm^{-2} (**2**), V_{oc} = 0.388 V (**1**) and 0.428 V (**2**) and FF = 0.452 (**1**) and 0.432 (**2**)]. It indicates the presence of CDCA as co-adsorbent shows 7 (**1**) and 3.2 (**2**) times higher efficiencies compared to absences of CDCA, which can prevent the formation of aggregation in the dyes when it was tightly packed with monolayer, and gives relatively better surface coverage and effectively hindering the back-electron transfer from conduction band of TiO_2 to electrolyte (iodide/triiodide). As a result, the improving the DSSC performance by enhancement of open circuit voltage of the device.[29,30] When compare to both the dyes **1** and **2**, 4-(cyanomethyl) benzoic acid (**2**) anchor showed higher photovoltaic performance than cyanoacrylic acid (**1**) anchor, because of introducing additional π-linkers and acceptor unit, which enable the lowering of the energy barrier and charge recombination process, it promotes

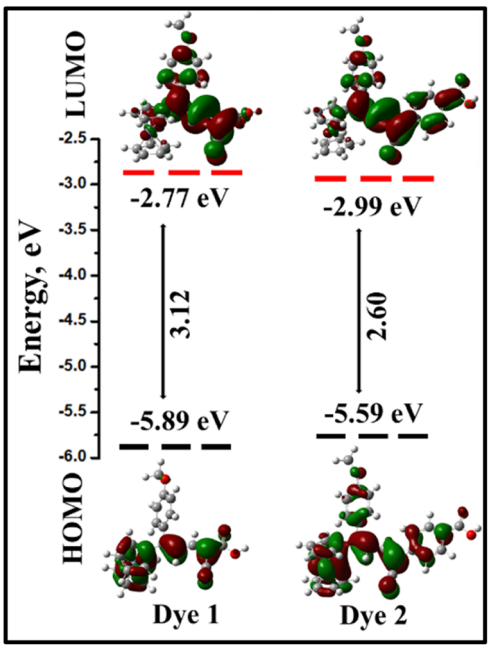

Fig. 8 Schematic energy levels of the dyes **1** and **2** at B3LYP/6-31+G(d,p)/LanL2TZf level of theory. Energy gaps and orbital distribution of HOMO and LUMO.

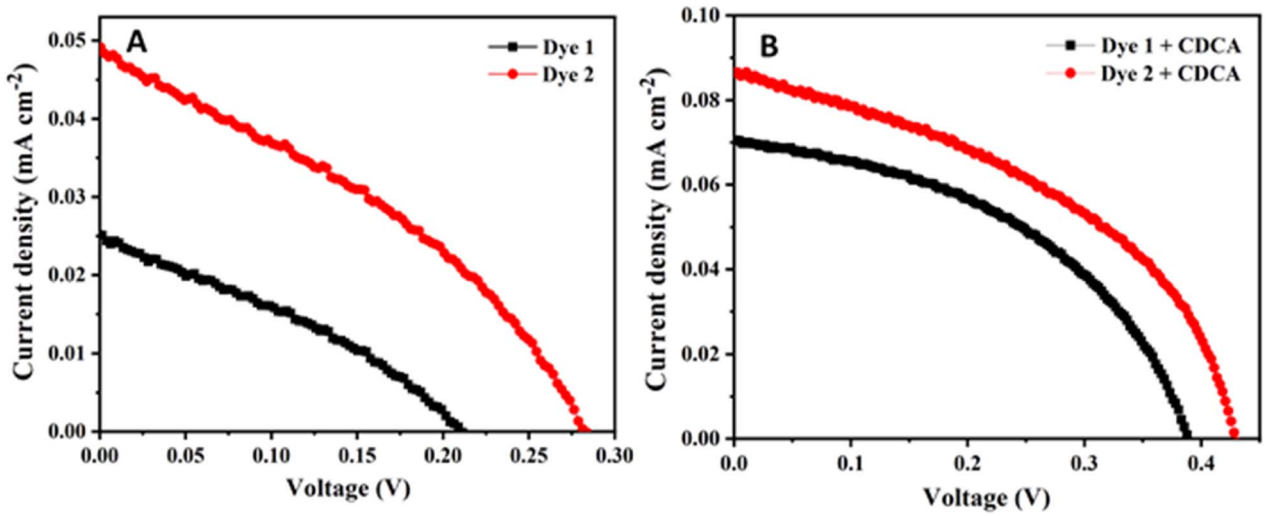

Fig. 9 *J–V* curves of ferrocene-based dyes **1** and **2** (A) without and (B) with co-adsorbent (CDCA) under 1 sun condition.

electron transport and high charge collection efficiency.[53] The 4-(cyanomethyl) benzoic acid (**2**) anchor have higher loading capability on the TiO_2 surface, which suppresses charge recombination and shows partially greater efficiencies than **1**. The dyes **1** and **2** shows low power conversion efficiency due to the low absorption observed in the visible region. The electron transfer between the acceptor and ferrocene was confirmed by the completely quenched fluorescence of the dyes, which leads low photon conversion efficiency.[54] An important reason for the poor performance of these solar cell by introduction of the methoxy phenyl group as an additional donor, which suppresses charge recombination as well as the dye regeneration process.[55] However, the power conversion efficiencies of the dyes were comparable with the obtained for a ferrocene-based porphyrin with a cobalt(II/III) electrolyte ($\eta = 0.0081\%$)[24] and ferrocene-modified zinc phthalocyanine using iodide/triiodide (I^-/I_3^-) electrolyte ($\eta = 0.003\%$).[54] Because, the addition of co-adsorbent of chenodeoxycholic acid (CDCA) prevent the formation of aggregation in the dyes when it was tightly packed with monolayer, and gives relatively better surface coverage and effectively hindering the back-electron transfer from conduction band of TiO_2 to electrolyte (iodide/triiodide). As a result, the improving the DSSC performance by enhancement of open circuit voltage (V_{oc}) of the device.[29]

3.7 Electrochemical impedance spectroscopy (EIS)

To investigate the electron transport properties of the TiO_2-dye-electrolyte interface in DSSCs, we have carried out electrochemical impedance spectroscopy (EIS). In EIS the study of the semicircle in the middle frequency region is associated with the electron/charge transfer at the TiO_2-dye-electrode interface.[26] The EIS of Nyquist and Bode plots for dyes **1** and **2** with and without CDCA are shown in Fig. 10. According to the Nyquist plot shown in Fig. 10A, the charge transfer resistance for the TiO_2-dye-electrolyte interface decreases with decreasing the semicircle diameter. The charge transfer resistance decreases with the dyes in the following order: **1** > **2** > **1** + CDCA > **2** + CDCA at the TiO_2-dye-electrolyte interface. The study of EIS spectra is in good agreement with the highest and lowest efficiency of the dyes.

The electron lifetime (τ_e) was calculated from the peak frequency (f_{peak}) in the frequency region corresponding to the TiO_2-dye-electrolyte interface in the Bode phase plot (Fig. 10B), according to the $\tau_e = 1/2\pi f_{peak}$.[23] The obtained values of electron lifetimes for the DSSCs based on **1** and **2** are 6.14 ms (for **1**) 6.53 ms (for **2**), 10.34 (for **1** + CDCA) and 10.61 ms (for **2** + CDCA) respectively, indicating that the back charge recombination is suppressed for the DSSC sensitized with CDCA as compared to without CDCA and the longer electron lifetimes of dye could explain the significant enhancement in V_{oc}.

Table 3 Photovoltaic parameters of DSSC based ferrocene dyes **1** and **2**

	Without CDCA					With CDCA[a]				
Dyes	J_{SC} (mA cm^{-2})	V_{OC} (V)	FF	η (%)	Dye loading without CDCA (mol cm^{-2})	J_{SC} (mA cm^{-2})	V_{OC} (V)	FF	η (%)	Dye loading with CDCA (mol cm^{-2})
Dye **1**	0.025	0.211	0.318	0.0017	0.253×10^{-7}	0.071	0.388	0.452	0.012	0.42×10^{-7}
Dye **2**	0.049	0.282	0.347	0.0047	0.37×10^{-7}	0.086	0.428	0.432	0.015	0.55×10^{-7}

[a] With chenodeoxycholic acid (CDCA) TiO_2 film has a 5 μm scattering layer and 6 μm transparent layer. Electrolyte composition: 0.05 M iodine, 0.1 M lithium iodide, 0.6 M 1-butyl-3-methylimidazolium iodide, and 0.5 M of *t*-butyl pyridine in 15 : 85 v/v % of valeronitrile and acetonitrile.

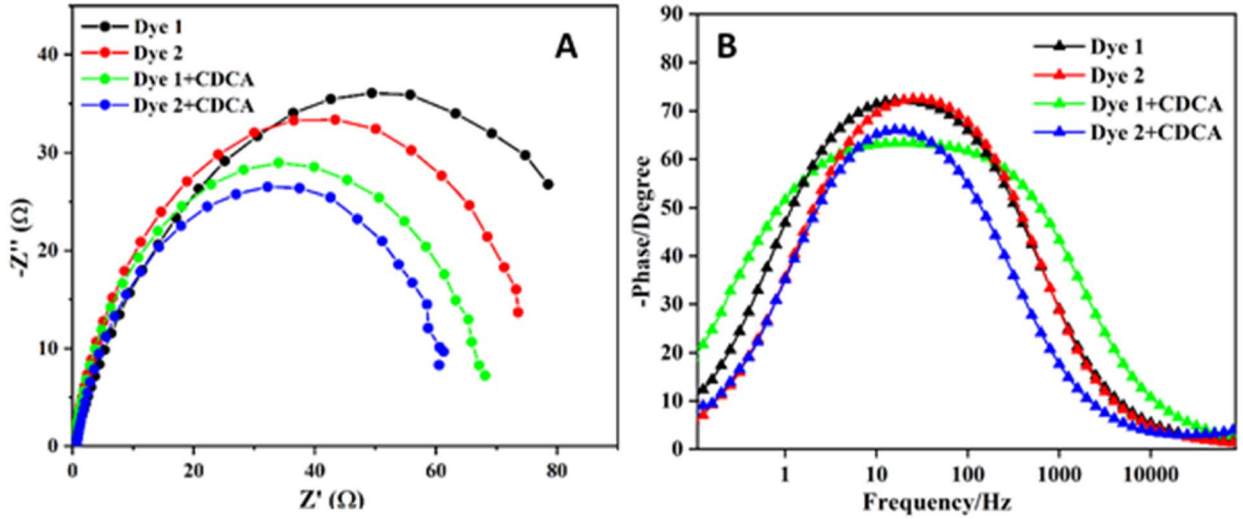

Fig. 10 Electrochemical impedance spectra of DSSCs measured at V_{oc}, 100 mWcm^{-2} (A) Nyquist plots (B) Bode plots.

4 Conclusion

In this present work, we have successfully synthesized new ferrocene conjugated linear multi-donor π-extended push–pull dyes **1** and **2**, and were spectroscopically characterized. The thermal stability of the dyes was stable around 180 °C for dye (**1**) and 240 °C for dye (**2**). The electronic absorption spectra for sensitizers showed improved intramolecular charge transfer (ICT) between the electron donor and acceptor, which creates an efficient charge separated state. In addition, the experimentally observed HOMO and LUMO values are in good agreement with the theoretical calculation by B3LYP/6-31+G(d,p)/LanL2TZf method. The photovoltaic performances of carboxylic anchor dyes **1** and **2** were carried out using with and without co-adsorbent, and utilized as a photosensitizer in TiO_2 based DSSCs. The obtained photovoltaic parameters of dye **2** are open-circuit voltage (V_{oc}) = 0.428, short-circuit current density (J_{sc}) = 0.086, the fill factor (FF) = 0.432 and the energy efficiencies (η) = 0.015%, the overall power conversion efficiencies were found to be increased in the presence of CDCA as a co-adsorbent. The addition of chenodeoxycholic acid (CDCA) as co-adsorbent, which shows higher efficiencies compared to absences of CDCA. Because, CDCA can prevent the formation of aggregation in the dyes and gives relatively better surface coverage and effectively hindering the back-electron transfer from conduction band of TiO_2 to electrolyte. Thus, significantly enhanced electron lifetime and suppresses electron recombination of the ferrocenyl multi-donor sensitizers, results improved J_{sc}, V_{oc} and η. Among the dyes, 4-(cyanomethyl) benzoic acid (**2**) anchor showed partially greater photovoltaic performance as compared with cyanoacrylic acid (**1**) anchor, due to the introduction of appropriate π-linkers and acceptor unit, which enable the lowering of the energy barrier and suppresses charge recombination process. The higher efficiencies can be achieved by extending the π-conjugation in the ferrocenyl D–π–A system, which absorbed more absorption in the visible region, it was currently in progress in our laboratory.

Conflicts of interest

There are no conflicts to declare.

Acknowledgements

We gratefully acknowledge the financial support from the DST Indo-Italian Joint Project (No. INT/Italy/P-15/2016(SP)). S. P. thanks Indian Council of Medical Research (ICMR) for the Senior Research Fellowship (SRF) [File No. 45/30/2020-BIO/BMS]. The authors thank VIT for providing "VIT SEED GRAND (File No. SG20210122)" for carrying out this research work. The authors gratefully acknowledge the VIT-SIF for providing the instrumental facilities. The authors thank Prof. Kothandaraman Ramanujam from the Department of Chemistry, Indian Institute of Technology Madras, Chennai and DST-IITM Solar Energy Harnessing Centre for DSSC performance.

References

1 B. O'Regan and M. Grätzel, A low-cost, high-efficiency solar cell based on dye-sensitized colloidal TiO_2 films, *Nature*, 1991, **353**, 737–740.
2 M. Grätzel, Recent advances in sensitized mesoscopic solar cells, *Acc. Chem. Res.*, 2009, **42**, 1788–1798.
3 A. Yella, C. L. Mai, S. M. Zakeeruddin, S. N. Chang, C. H. Hsieh, C. Y. Yeh and M. Grätzel, Molecular engineering of push-pull porphyrin dyes for highly efficient dye-sensitized solar cells: The role of benzene spacers, *Angew. Chem., Int. Ed.*, 2014, **126**, 3017–3021.
4 L. Y. Han, A. Islam, H. Chen, C. Malapaka, B. Chiranjeevi, S. F. Zhang, X. D. Yang and M. Yanagida, High-efficiency

dye-sensitized solar cell with a novel co-adsorbent, *Energy Environ. Sci.*, 2012, **5**, 6057–6060.

5 B. O'Regan, K. Walley, M. Juozapavicius, A. Anderson, F. Matar, T. Ghaddar, S. M. Zakeeruddin, C. Klein and J. R. Durrant, Structure/function relationships in dyes for solar energy conversion: a two-atom change in dye structure and the mechanism for its effect on cell voltage, *J. Am. Chem. Soc.*, 2009, **131**, 3541–3548.

6 F. Gao, Y. Wang, D. Shi, J. Zhang, M. Wang, X. Jing, R. Humphry-Baker, P. Wang, S. M. Zakeeruddin and M. Gratzel, Enhance the optical absorptivity of nanocrystalline TiO2 film with high molar extinction coefficient ruthenium sensitizers for high performance dye-sensitized solar cells, *J. Am. Chem. Soc.*, 2008, **130**, 10720–10728.

7 D. Kuang, S. Ito, B. Wenger, C. Klein, J. E. Moser, R. Humphry-Baker, S. M. Zakeeruddin and M. Gratzel, High molar extinction coefficient heteroleptic ruthenium complexes for thin film dye-sensitized solar cells, *J. Am. Chem. Soc.*, 2006, **128**, 4146–4154.

8 C. Y. Chen, M. Wang, J. Y. Li, N. Pootrakulchote, L. Alibabaei, C. H. Ngoc-le, J. D. Decoppet, J. H. Tsai, C. Grätzel, C. G. Wu and S. M. Zakeeruddin, Highly efficient light-harvesting ruthenium sensitizer for thin-film dye-sensitized solar cells, *ACS Nano*, 2009, **3**, 3103–3109.

9 S. Aghazada, P. Gao, A. Yella, G. Marotta, T. Moehl, J. Teuscher, J. E. Moser, F. De Angelis, M. Grätzel and M. K. Nazeeruddin, Ligand engineering for the efficient dye-sensitized solar cells with ruthenium sensitizers and cobalt electrolytes, *Inorg. Chem.*, 2016, **55**, 6653–6659.

10 Y. Huang, W. C. Chen, X. X. Zhang, R. Ghadari, X. Q. Fang, T. Yu and F. T. Kong, Ruthenium complexes as sensitizers with phenyl-based bipyridine anchoring ligands for efficient dye-sensitized solar cells, *J. Mater. Chem. C*, 2018, **6**, 9445–9452.

11 H. Yin, S. Chen, S. H. Cheung, H. W. Li, Y. Xie, S. W. Tsang, X. Zhu and S. K. So, Porphyrin-based thick-film bulk-heterojunction solar cells for indoor light harvesting, *J. Mater. Chem. C*, 2018, **6**, 9111–9118.

12 H. Choi, S. Paek, N. Lim, Y. H. Lee, M. K. Nazeeruddin and J. Ko, Efficient perovskite solar cells with 13.63% efficiency based on planar triphenylamine hole conductors, *Chem. – Eur. J.*, 2014, **20**, 10894–10899.

13 A. Magomedov, E. Kasparavičius, K. Rakstys, S. Paek, N. Gasilova, K. Genevičius, G. Juška, T. Malinauskas, M. K. Nazeeruddin and V. Getautis, Pyridination of hole transporting material in perovskite solar cells questions the long-term stability, *J. Mater. Chem. C*, 2018, **6**, 8874–8878.

14 Z. Yang, C. Shao and D. Cao, Screening donor groups of organic dyes for dye-sensitized solar cells, *RSC Adv.*, 2015, **5**, 22892–22898.

15 M. Liang and J. Chen, Arylamine organic dyes for dye-sensitized solar cells, *Chem. Soc. Rev.*, 2013, **42**, 3453–3488.

16 Y. Ooyama and Y. Harima, Molecular designs and syntheses of organic dyes for dye-sensitized solar cells, *Eur. J. Org. Chem.*, 2009, **18**, 2903–2934.

17 P. Stepnicka, *Ferrocenes: Ligands, Materials and Biomolecules*, John Wiley and Sons Ltd., 2008.

18 A. Auger and J. C. Swarts, Synthesis and group electronegativity implications on the electrochemical and spectroscopic properties of diferrocenyl meso-substituted porphyrins, *Organometallics*, 2007, **26**, 102–109.

19 J. Conradie, T. S. Cameron, M. A. S. Aquino, G. J. Lamprecht and J. C. Swarts, Synthetic, electrochemical and structural aspects of a series of ferrocene-containing dicarbonyl β-diketonato rhodium(I) complexes, *Inorg. Chim. Acta*, 2005, **358**, 2530–2542.

20 A. Ghosh, S. Mishra, S. Giri, S. M. Mobin, A. Bera and S. Chatterjee, Electrolyte-free dye-sensitized solar cell with high open circuit voltage using a bifunctional ferrocene-based cyanovinyl molecule as dye and redox couple, *Organometallics*, 2018, **37**, 1999–2002.

21 V. Singh, R. Chauhan, A. N. Gupta, V. Kumar, M. G. B. Drew, L. Bahadur and N. Singh, Photosensitizing activity of ferrocenyl bearing Ni (II) and Cu (II) dithiocarbamates in dye sensitized TiO_2 solar cells, *Dalton Trans.*, 2014, **43**, 4752–4761.

22 R. Yadav, M. Trivedi, G. Kociok-Kohn, R. Chauhan, A. Kumar and S. W. Gosavi, Ferrocenyl Dithiocarbamate Based d^{10} Transition-Metal Complexes as Potential Co-Sensitizers in Dye-Sensitized Solar Cells, *Eur. J. Inorg. Chem.*, 2016, **7**, 1013–1021.

23 R. Misra, R. Maragani, K. R. Patel and G. D. Sharma, Synthesis, optical and electrochemical properties of new ferrocenyl substituted triphenylamine based donor–acceptor dyes for dye sensitized solar cells, *RSC Adv.*, 2014, **4**, 34904–34911.

24 D. Sirbu, C. Turta, A. C. Benniston, F. Abou-Chahine, H. Lemmetyinen, N. V. Tkachenko, C. Woodd and E. Gibson, Synthesis and properties of a meso-tris–ferrocene appended zinc (II) porphyrin and a critical evaluation of its dye sensitised solar cell (DSSC) performance, *RSC Adv.*, 2014, **4**, 22733–22742.

25 Y. Patil, R. Misra, M. K. Singh and G. D. Sharma, Ferrocene-diketopyrrolopyrrole based small molecule donors for bulk heterojunction solar cells, *Phys. Chem. Chem. Phys.*, 2017, **19**, 7262–7269.

26 R. Yadav, A. Singh, G. Kociok-Kohn, R. Chauhan, A. Kumar and S. Gosavi, Ferrocenyl benzimidazole with carboxylic and nitro anchors as potential sensitizers in dye-sensitized solar cells, *New J. Chem.*, 2017, **41**, 7312–7321.

27 R. Chauhan, M. Shahid, M. Trivedi, D. P. Amalnerkar and A. Kumar, Dye-Sensitized Solar Cells with Biferrocenyl Antennae Having Quinoxaline Spacers, *Eur. J. Inorg. Chem.*, 2015, **22**, 3700–3707.

28 M. Cariello, S. Ahn, K.-W. Park, S. K. Chang, J. Hong and G. Cooke, An investigation of the role increasing π-conjugation has on the efficiency of dye-sensitized solar cells fabricated from ferrocene-based dyes, *RSC Adv.*, 2016, **6**, 9132–9138.

29 J. Li, W. Wu, J. Yang, J. Tang, Y. Long and J. Hua, Effect of chenodeoxycholic acid (CDCA) additive on phenothiazine

dyes sensitized photovoltaic performance, *Sci. China: Chem.*, 2011, **54**, 699–706.

30 B. Nagarajan, S. Kushwaha, R. Elumalai, S. Mandal, K. Ramanujam and D. Raghavachari, Novel ethynyl-pyrene substituted phenothiazine based metal free organic dyes in DSSC with 12% conversion efficiency, *J. Mater. Chem. A*, 2017, **5**, 10289–10300.

31 D. Unny, G. R. Kandregula and K. Ramanujam, Starburst configured imidazole-arylamine organic sensitizers for DSSC applications, *J. Photochem. Photobiol., A*, 2022, **426**, 113735.

32 S. Prabu and N. Palanisami, Aggregation induced emission (AIE)-active ferrocene conjugated linear π-extended multi donor–π–acceptor (D–D′–π–A) chromophores: synthesis, structural, theoretical, linear and nonlinear optical studies, *Dyes Pigm.*, 2022, **201**, 110193.

33 A. M. El-Zohry, J. Cong, M. Karlsson, L. Kloo and B. Zietz, Ferrocene as a rapid charge regenerator in dye-sensitized solar cells, *Dyes Pigm.*, 2016, **132**, 360–368.

34 W. Sharmoukh, J. Cong, B. A. Ali, N. K. Allam and L. Kloo, Comparison between benzothiadizole-thiophene-and benzothiadizole-furan-based D–A–π–A dyes applied in dye-sensitized solar cells: Experimental and theoretical insights, *ACS Omega*, 2020, **5**, 16856–16864.

35 D. M. Almenningen, V. M. Engh, E. A. Strømsodd, H. E. Hansen, A. F. Buene, B. H. Hoff and O. R. Gautun, Synthetic efforts to investigate the effect of planarizing the triarylamine geometry in dyes for dye-sensitized solar cells, *ACS Omega*, 2022, **7**, 22046–22057.

36 M. Hisatome, S. Koshikawa, K. Chimura, H. Hashimoto and K. Yamakawa, Organometallic compounds XXVIII. Intermolecular carbon-carbon bond formation by oxidation of (1-arylvinyl) ferrocenes with molecular oxygen in the presence of silica gel, *J. Organomet. Chem.*, 1978, **145**, 225–239.

37 C. Lee, W. Yang and R. G. Parr, Development of the Colle-Salvetti correlation-energy formula into a functional of the electron density, *Phys. Rev. B: Condens. Matter Mater. Phys.*, 1988, **37**, 785.

38 R. G. Parr and Y. Weitao, *Density-Functional Theory of Atoms and Molecules*, Oxford University Press, Oxford, 1994.

39 M. Toma, T. Kuvek and V. Vrček, Ionization energy and reduction potential in ferrocene derivatives: comparison of hybrid and pure DFT functionals, *J. Phys. Chem. A*, 2020, **124**, 8029–8039.

40 M. J. Frisch, G. W. Trucks, H. B. Schlegel, G. E. Scuseria, M. A. Robb, J. R. Cheeseman, G. Scalmani, V. Barone, B. Mennucci, G. A. Petersson, H. Nakatsuji, M. Caricato, X. Li, H. P. Hratchian, A. F. Izmaylov, J. Bloino, G. Zheng, J. L. Sonnenberg, M. Hada, M. Ehara, K. Toyota, R. Fukuda, J. Hasegawa, M. Ishida, T. Nakajima, Y. Honda, O. Kitao, H. Nakai, T. Vreven, J. A. Montgomery, J. E. Peralta, F. Ogliaro, M. Bearpark, J. J. Heyd, E. Brothers, K. N. Kudin, V. N. Staroverov, R. Kobayashi, J. Normand, K. Raghavachari, A. Rendell, J. C. Burant, S. S. Iyengar, J. Tomasi, M. Cossi, N. Rega, J. M. Millam, M. Klene, J. E. Knox, J. B. Cross, V. Bakken, C. Adamo, J. Jaramillo, R. Gomperts, R. E Stratmann, O. Yazyev, A. J. Austin, R. Cammi, C. Pomelli, J. W. Ochterski, R. L. Martin, K. Morokuma, V. G. Zakrzewski, G. A. Voth, P. Salvador, J. J. Dannenberg, S. Dapprich, A. D. Daniels, O. Farkas, J. B. Foresman, J. V. Ortiz, J. Cioslowski and D. J. Fox, *Gaussian16 Rev. C.01*, Gaussian, Inc., Wallingford CT, 2009.

41 R. D. Dennington, T. A. Keith and J. Millam, *GaussView Version 6.1.16*, Semichem Inc., Shawnee Mission. KS, 2016.

42 K. Senthilkumar, M. Pizzotti, K. Thirumoorthy, G. Di Carlo, S. Righetto, A. Orbelli Biroli, M. Haukka and N. Palanisami, New internal-charge-transfer second-order nonlinear optical chromophores based on the donor ferrocenyl pyrazole moiety, *J. Phys. Chem. C*, 2016, **120**, 20277–202311.

43 Y. S. Sohn, D. N. Hendrickson and H. B. Gray, Electronic structure of metallocenes, *J. Am. Chem. Soc.*, 1971, **93**, 3603–3612.

44 R. Chauhan, R. Yadav, A. K. Singh, M. Trivedi, G. Kociok-Köhn, A. Kumar, S. Gosavi and S. Rane, Ferrocenyl chalcones with phenolic and pyridyl anchors as potential sensitizers in dye-sensitized solar cells, *RSC Adv.*, 2016, **6**, 97664–97675.

45 L. Zhang and J. M. Cole, Dye aggregation in dye-sensitized solar cells, *J. Mater. Chem. A*, 2017, **5**, 19541–19559.

46 S. Prabu, E. David, T. Viswanathan, J. S. A. Jinisha, R. Malik, K. R. Maiyelvaganan, M. Prakash and N. Palanisami, Ferrocene conjugated donor–π–acceptor malononitrile dimer: Synthesis, theoretical calculations, electrochemical, optical and nonlinear optical studies, *J. Mol. Struct.*, 2020, **1202**, 127302.

47 M. Gopalakrishnan and N. Palanisami, New sterically hindered tin (IV) siloxane precursors to tinsilicate materials: synthesis, spectral, structural and photocatalytic studies, *RSC Adv.*, 2016, **6**, 1760–1768.

48 E. David, K. Thirumoorthy and N. Palanisami, Ferrocene-appended donor–π–acceptor Schiff base: Structural, nonlinear optical, aggregation-induced emission and density functional theory studies, *Appl. Organomet. Chem.*, 2018, **32**, e4522.

49 C. M. Cardona, W. Li, A. E. Kaifer, D. Stockdale and G. C. Bazan, Electrochemical considerations for determining absolute frontier orbital energy levels of conjugated polymers for solar cell applications, *Adv. Mater.*, 2011, **23**, 2367–2371.

50 S. Prabu and N. Palanisami, Ferrocene appended Y-shaped imidazole aldehyde chromophores: Synthesis, the effect of alkyl chain in the second order nonlinear optical properties and theoretical studies, *J. Mol. Struct.*, 2022, **1264**, 133137.

51 A. Singh, A. Dutta, D. Srivastava, G. Kociok-Köhn, R. Chauhan, S. W. Gosavi, A. Kumar and M. Muddassir, Effect of different aromatic groups on photovoltaic performance of 1, 1′-bis (diphenylphosphino) ferrocene functionalized Ni (II) dithiolates as sensitizers in dye sensitized solar cells, *Appl. Organomet. Chem.*, 2021, **35**, e6402.

52 A. F. Buene, D. M. Almenningen, A. Hagfeldt, O. R. Gautun and B. H. Hoff, First report of chenodeoxycholic acid-substituted dyes improving the dye monolayer quality in dye-sensitized solar cells, *Sol. RRL*, 2020, **4**, 1900569.

53 Q. Wang, J. E. Moser and M. Gratzel, Electrochemical impedance spectroscopic analysis of dye-sensitized solar cells, *J. Phys. Chem. B*, 2005, **109**, 14945–14953.

54 M. S. An, S. W. Kim and J. D. Hong, Synthesis and characterization of peripherally ferrocene-modified zinc phthalocyanine for dye-sensitized solar cell, *Bull. Korean Chem. Soc.*, 2010, **31**, 3272–3278.

55 D. Koteshwar, S. Prasanthkumar, S. P. Singh, T. H. Chowdhury, I. Bedja, A. Islam and L. Giribabu, Effects of methoxy group (s) on D–π–A porphyrin based DSSCs: efficiency enhanced by co-sensitization, *Mater. Chem. Front.*, 2022, **6**, 580–592.